metals

MDPI

Article

Development of Amplifier Circuit by Active-Dummy Method for Atmospheric Corrosion Monitoring in Steel Based on Strain Measurement

Nining Purwasih [1,2,*], Naoya Kasai [1], Shinji Okazaki [3] and Hiroshi Kihira [4]

1 Department of Risk Management and Environmental Sciences, Graduate School of Environmental and Information Sciences, Yokohama National University, Yokohama 240-8501, Japan; kasai-naoya-pf@ynu.ac.jp
2 Department of Electrical Engineering, Faculty of Engineering, Lampung University, Bandar Lampung 35141, Indonesia
3 Division of Material Science and Engineering, Graduate School of Engineering, Yokohama National University, Yokohama 240-8501, Japan; okazaki-shinji-yp@ynu.ac.jp
4 Nippon Steel & Sumikin Research Institute, Tokyo 100-0005, Japan; kihira.hiroshi@nsri.nssmc.com
* Correspondence: nining-purwasih-gf@ynu.jp; Tel.: +81-45-339-3979

Received: 31 October 2017; Accepted: 18 December 2017; Published: 22 December 2017

Abstract: This paper describes an amplifier circuit fabricated by the active-dummy method for atmospheric corrosion monitoring based on strain measurement. The circuit was used to determine the relationship between the voltage and strain. Experiments involving the thickness reduction of low-carbon steel test pieces induced by galvanostatic electrolysis were carried out with the amplifier circuit. The circuit was capable of accurately measuring signals induced by the thickness reduction of the test piece. Moreover, the circuit was assessed for the effects of environmental temperature drift, and was found to exhibit a high tolerance. The proposed amplifier circuit would be suitable for atmospheric corrosion monitoring in many types of infrastructure.

Keywords: atmospheric corrosion monitoring sensor; steel test piece; strain measurement; master curve; galvanostatic electrolysis

1. Introduction

Corrosion damages the steel that is used for many types of infrastructure. It causes significant damage to steel, which can lead to catastrophic structural failure. Based on this, corrosion detection on steel structures is necessary. There is a great deal of research on how to detect corrosion, such as using a radio-frequency identification (RFID) sensor [1–3] and the methods involving optic fibers [4–8]. These methods are all effective in ensuring the safety level of steel structures.

Atmospheric corrosion monitoring is also important in predicting the corrosion damage of steel structures. Factors governing atmospheric corrosion are the temperature, dew, precipitation, relative humidity, and nitrate, chloride, and sulfate ions. At high temperatures, some electrolytes become highly reactive. Dew, precipitation, and relative humidity also have a large effect on the corrosion process. Nitrate, chloride, and sulfate ions can increase the corrosiveness of the environment. All these factors require further elaboration in order to clearly describe the phenomenon of atmospheric corrosion.

Several conventional methods for atmospheric corrosion monitoring, such as weight and thickness loss [9–16], polarization resistance [17], the corrosion behavior of steels with different nickel content [18,19], stainless steels [20], galvanized steel [21,22], zinc [23], and electrochemical impedance spectroscopy [24–29], have been extensively used to monitor atmospheric corrosion. Recent developments for monitoring atmospheric corrosion including using electric resistance sensors [30,31], pulsed Eddy current testing (ECT) [32], and passive wireless sensors [33]. In addition to new methods,

in order to develop the atmospheric corrosion monitoring (ACM) sensor, many researchers also investigated various characteristics of corrosion. These included metal loss, material characteristics of corrosion layers [34] which were analyzed using different analysis methods, such as finite element analysis (FEA) models that used two layers of the corrosion layer and test piece [7,30], microscopic analysis [5,28], and X-ray diffraction [6,25,26]. In addition to these techniques, electrochemical methods are useful because they allow in situ corrosion monitoring [35]. However, precise monitoring is difficult because electrochemical methods are very sensitive to the corrosion reactions. Once an electrode begins to corrode, the redox reactions of the corrosion products affect the current density signals. In the case of steel, ferrous and ferric ions coexist in the corrosion product. These factors ultimately prevent precise evaluation of atmospheric corrosion. Thus, a highly-accurate in situ sensor capable of monitoring atmospheric corrosion is needed.

Against this background, we have developed a new principle for measuring corrosion rates in real-time. A highly-accurate in situ sensor, capable of atmospheric corrosion monitoring by measuring the thickness of carbon steel, is proposed. Previous research on in situ monitoring of thinning of test pieces by galvanostatic electrolysis [36] has shown that strain can provide a measure of the reduction in thickness due to corrosion. However, in actual applications, there is significant noise due to variations in temperature and other factors during field measurements.

Therefore, the purpose of this study is to develop an amplifier circuit for atmospheric corrosion monitoring based on strain measurement by using the active-dummy method, which has high sensitivity and can reduce the effect of temperature on the measurement environment. A dummy circuit compensated for the temperature drift in the signal with an active circuit was successfully designed, and experiments involving galvanostatic electrolysis were conducted by using the amplifier circuits to determine the thinning of test pieces through strain measurements. In addition, the effect of the temperature on the measurement environment on the signals, was investigated.

2. Materials and Methods

2.1. Design of Amplifier Circuit by Active-Dummy Method

2.1.1. Principle of ACM (Atmospheric Corrosion Monitoring) Sensor Based on Strain Measurement

The mechanism whereby the ACM sensor can measure the thinning of test pieces is shown in Figure 1. A test piece with a thickness y is subjected to a bending moment M; the radius of the curvature of the test piece is denoted by ρ, and the center angle by $\mathrm{d}\theta$. Line segment O-O represents the neutral plane, and its length is the unaltered by the deformation. Line segment A-A is shortened upon deformation and its length is equal to $(\rho - \frac{y}{2})\,\mathrm{d}\theta$. The strain on the A-A surface can be expressed by [35]:

$$\varepsilon = \frac{(\rho - \frac{y}{2})\mathrm{d}\theta - \rho\mathrm{d}\theta}{\rho\mathrm{d}\theta} = -\frac{y}{2\rho} \quad (1)$$

When the test piece thickness is reduced as a result of corrosion, the distance between the neutral plane and the surface of the test piece decreases, as seen in Figure 1. From Equation (1), the change in strain is expressible as:

$$\Delta\varepsilon = -\frac{\Delta y}{2\rho} \text{ and } \Delta y = -2\rho\,\Delta\varepsilon \quad (2)$$

The change in the test piece thickness under a constant ρ can be measured by the change in strain of the concave surface. Through Equation (2), we can monitor the diminishing thickness of the test piece by monitoring the change in strain.

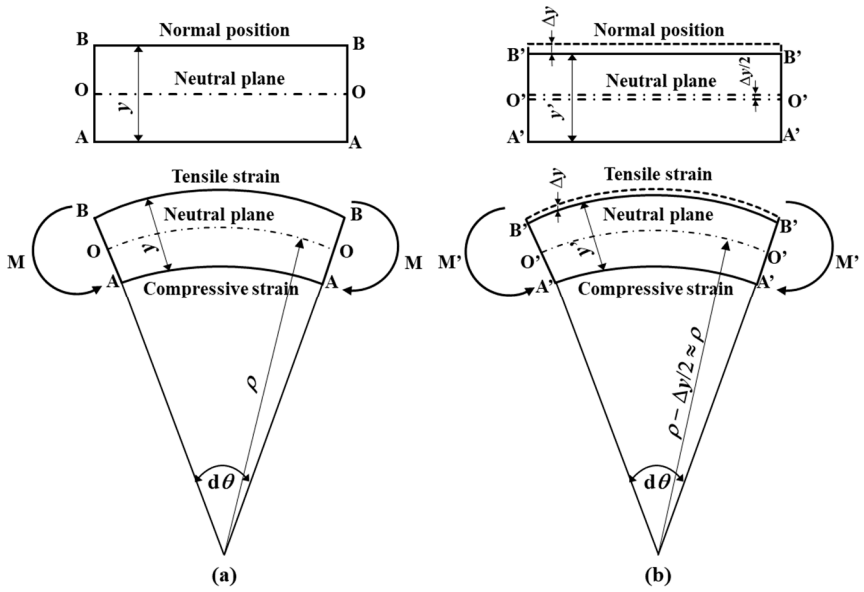

Figure 1. Schematic of test piece subjected to moments M and M′. (**a**) Initial conditions; (**b**) after the test piece thickness decreases upon corrosion.

2.1.2. Concept of Amplifier Circuit by Active-Dummy Method

The amplifier circuit fabricated by the active-dummy method for atmospheric corrosion monitoring consists of bridge circuits with strain gauge sensors connected to the test piece, pre-amplifier circuits based on an instrumentation stage operational amplifier with a circuit identical to that used in the active-dummy method, and a differential circuit that differs from the active-dummy circuit. The design concept of the amplifier circuit used in the active-dummy method to monitor atmospheric corrosion is illustrated in Figure 2. $\varepsilon_{\mu,\tau,o}$ is the strain with input from the signal and environmental factor. ε_{μ} is the strain from the thinning of the test piece due to corrosion stress. $\varepsilon_{\tau,o}$ is the strain due to environmental effects, such as temperature and humidity. The active circuit has not only ε_{μ} but also $\varepsilon_{\tau,o}$ as inputs, whereas in the case of the dummy circuit, the only input is $\varepsilon_{\tau,o}$. The differential circuit subtracts the output from the active circuit from the output from the dummy circuit. Since the dummy circuit compensates for the effects of environmental or atmospheric conditions on the active circuit, an accurate value is obtained for ε_{m}.

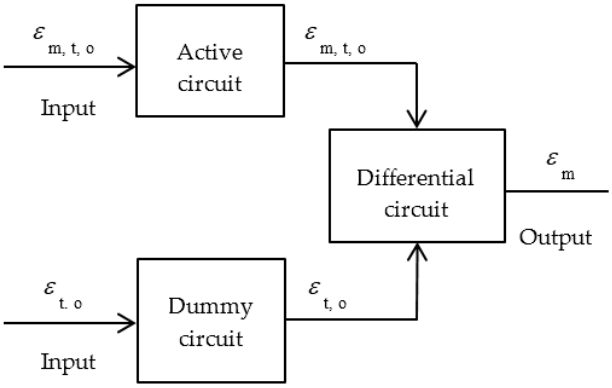

Figure 2. Design concept of the active-dummy method.

2.2. Experimental Setup

2.2.1. Design of ACM Sensor

The test piece was 95 mm in length, 45 mm in width, 0.48 mm in thickness, and made of low-carbon steel. To remove the residual stress, the test piece was heat-treated at 450 °C for 1 h. A corroded area, 30 mm in length and 30 mm in width, was arranged in the center of the test piece with no plastic coating, while the remaining area was coated with plastic to prevent corrosion (in other words, an uncorroded area), as shown in Figure 3. The corroded area which becomes thinner as a result of corrosion, enables the calculation of the reduction in thickness. To calculate the radius of the curvature of the apparatus, ρ, Hooke's law and Equation (1) can be combined, yielding the equation:

$$\rho = \frac{Ey}{2\sigma_y} \tag{3}$$

By using a yield stress of 240 MPa, a Young's modulus of 210 GPa [34], and a test piece thickness of 0.5 mm, ρ in the elastic deformation range was calculated via Equation (3) to be 219 mm. To prevent local plastic deformation of the test piece, ρ should be roughly twice this value. Thus, ρ = 430 mm.

The apparatus comprises a base and cover made of polyvinyl chloride, as shown in Figure 3. According to [34], $\Delta y = 0.86 \times \Delta\varepsilon$. The units of $\Delta\varepsilon$ are με (μm/m), the units of Δy are μm, and the units of the coefficient 0.86 are m/ε. A strain gauge, which was in contact with the back of the test piece, was installed in the apparatus.

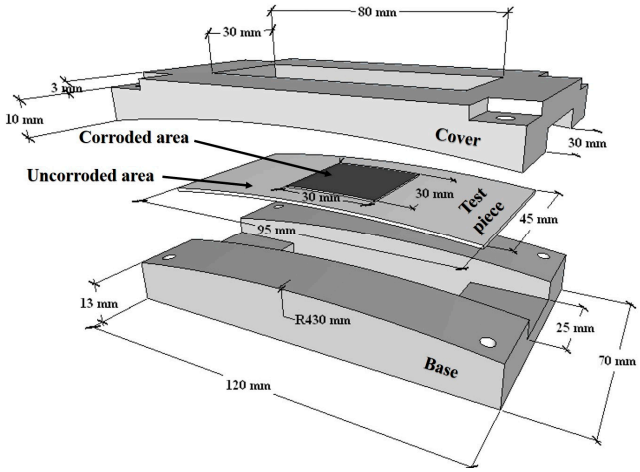

Figure 3. Test piece and apparatus for ACM (atmospheric corrosion monitoring) sensor. The apparatus comprises of a base, test piece, and cover. A corroded area, 30 mm in length and 30 mm in width, was formed at the center of the test piece; the remaining area was uncorroded.

2.2.2. Strain Gauge Configuration of Test Piece for Active and Dummy Circuit

The test piece for the active circuit is TP_A, and the test piece for the dummy circuit is TP_D. TP_A has active and dummy strain gauges at positions 1 and 3, and a strain gauge for the commercial strain measurement device at position 1. TP_D has active and dummy strain gauges at positions 2 and 3. TP_A has a 900 mm^2 corroded area at the center of the test piece; the remaining area is uncorroded. TP_D only has a corroded area. The configuration of the strain gauges on the test piece is shown in Figure 4. Position 1 is at the center of the active test piece with curvature ρ, and has active gauges (R_{AA}) on the back of the corrosion area. Position 2 is at the center of the dummy test piece with curvature ρ, and has active gauges (R_{AD}) on the back of the uncorroded area. Position 3 is at the edge of both test pieces on the back of the uncorroded area, and has dummy strain gauges (R_{DA} and R_{DD}). The first letter in the subscript denotes whether the gauge is active or dummy, while the second letter denotes

whether the circuit is active or dummy. R_{AA} is placed at the center of TP_A with curvature ρ to exert a stress on the strain gauges, as well as on the back of the corroded area in order to receive signals from the corrosion-induced thinning of the test piece. R_{DA} is placed at the edge of TP_A and on the back of the corroded area without stress to compensate for the effects of atmospheric conditions on the active gauge. R_{AD} and R_{DD}, as identical gauges of the active circuit, compensated for the active circuit and are placed in the uncorroded area on TP_D. S_G is the strain gauge for measuring the strain in the corroded area with a commercial strain meter and is placed at the center of the corroded area without bending. The strain gauges and their functions are shown in Table 1.

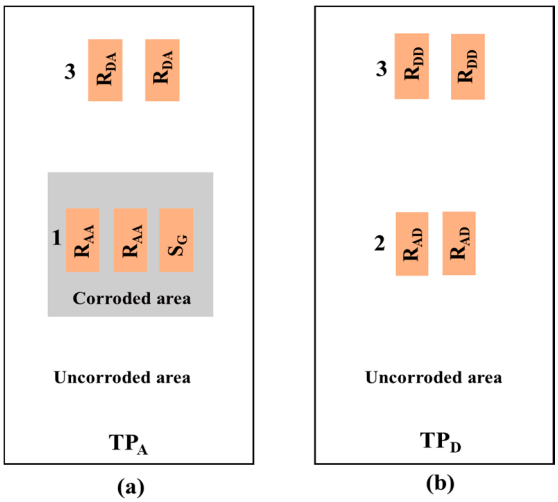

Figure 4. Configuration of strain gauges on test piece for ACM sensor. (**a**) TP_A with 900 mm^2 corroded area at the center and the remaining area uncorroded; (**b**) TP_D, with the entire test piece uncorroded.

Table 1. Position and purpose of strain gauges in Figure 4.

Positions of Strain Gauges	Active Circuit	Dummy Circuit
Active Strain Gauge	R_{AA}: Corroded area with bending. Detects signals due to corrosion-induced thinning of test piece.	R_{AD}: Uncorroded without bending. Detects signals without thinning of test piece.
Dummy Strain Gauge	R_{DA}: Uncorroded area without bending. Compensates for effects of environmental conditions on R_{AA}.	R_{DD}: Uncorroded area without bending. Compensates for effects of environmental conditions on R_{AD}.
Strain Gauge	SG: At the center of corroded area without bending. Measures the strain in the corroded area with commercial strain measurement device.	

2.2.3. Design of the Amplifier Circuit with the Active-Dummy Method

The amplifier circuit used in the active-dummy method (see Figure 5), with its gain of 10,000, was designed to measure very small strains of Tokyo Sokki FLA-5-11 strain gauges (Tokyo Sokki Kenkyujo Co., Ltd., Tokyo, Japan) when it was placed in a bridge circuit, such that R_{AA}, R_{DA}, R_{AD} and R_{DD}, all have the same resistance of 120 Ω. Using a voltage input (V_{IN}) of 3 V to adjust the current through the strain gauge, the output voltages of (i) the active bridge circuit, V_{BA}, (ii) the dummy bridge circuit, V_{BD}, (iii) the active circuit, V_A, (iv) the dummy circuit, V_D, and (v) the amplifier circuit, ΔV, should all be zero under balanced conditions. When a variation in the strain gauge resistance appeared in the signal, V_{BA} appeared and, when amplified, became V_A, in addition to ΔV also appearing. The input for the operational amplifier V_{CC} and V_{EE} is 10 V and became the maximum voltage of the circuit. To reduce the noise, capacitors were used as a filters in the input area, as well as a filter consisting of capacitors and resistors in the output area. INA128 op-amplifiers (Texas Instruments, Dallas, TX, USA), which are largely unaffected by temperature variations, were used. The other components had low

coefficients of thermal expansion and low tolerance. Figure 6 illustrates an amplifier circuit built by the present active-dummy method.

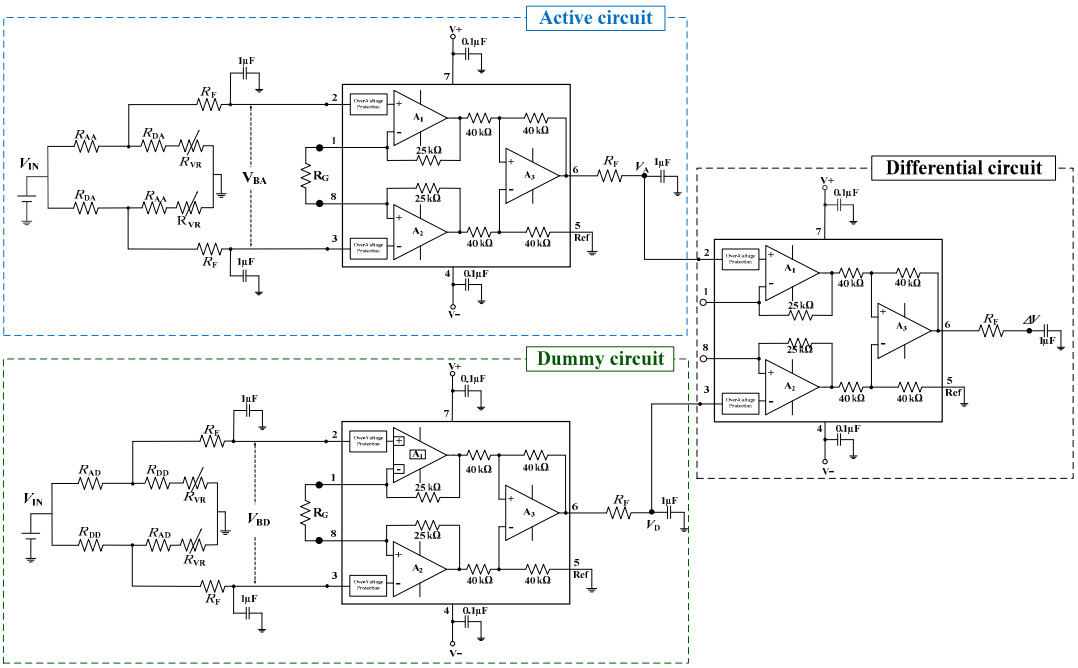

Figure 5. Design of the amplifier circuit by the active-dummy method.

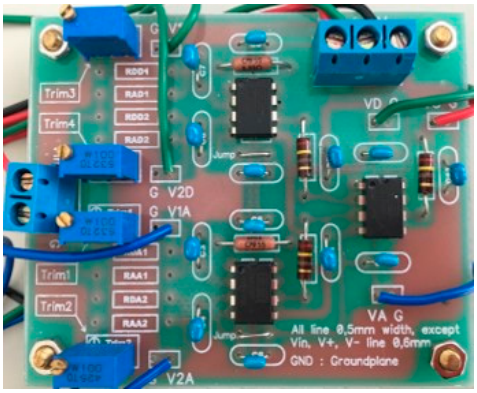

Figure 6. Photograph of the amplifier circuit by the active-dummy method.

2.2.4. Master Curve of the Strain-Voltage Relationship

This experiment employed a Graphtec GL7000 data logger (Graphtec Co., Yokohama, Japan) to monitor the voltage from the amplifier circuit and the temperature of the measurement environment, and a Kyowa Sensor Interface PCD-300B (Kyowa Electronic Instruments Co., Ltd., Tokyo, Japan) to measure the strain.

To induce a strain on TP_A, the edge of the test piece was fixed, and different weights were attached to the edge of the test piece. The center of the test piece exhibited a strain due to bending. Within the elastic strain region of the test piece, the relationship between strain and weight was linear. Meanwhile, the TP_D did not detect the variations in strain, only the behavior of the environment.

The output voltages of the active circuit, dummy circuit, and amplifier circuit were measured by taking data at a rate of 1 sample/s. S_G, which has the same position as R_{AA}, was modified from the

cantilever position using a balance. S_G, V_A, and V_S change simultaneously as the balance is moved. The balance was modified every 50 g to get the variation in the data up to the 10 V maximum.

2.2.5. In Monitoring of Thinning of Test Piece by Galvanostatic Electrolysis

This experiment was carried out to investigate the accuracy of the amplifier circuit using the active-dummy method, as described in Section 2.1.2. Figure 7 shows the experimental setup used to measure the change in strain due to the thinning of the TP_A of the ACM sensor through galvanostatic electrolysis. The electrolytic solution in the reservoir was 1 mol·L^{-1} hydrochloric acid solution. The working electrode was TP_A, and the counter electrode consisted of the same material as TP_A. The thickness of the working electrode was reduced by galvanostatic electrolysis with a current of 1 A, and the strain of the test piece was measured to assess the change in thickness. The corroded area was 900 mm^2. The difference in weight (ΔW) and thickness (Δy_A) of the test piece of the working electrode before and after the experiment were also measured. The data sampling interval was 30 s. TP_D was set in the apparatus, near the reservoir.

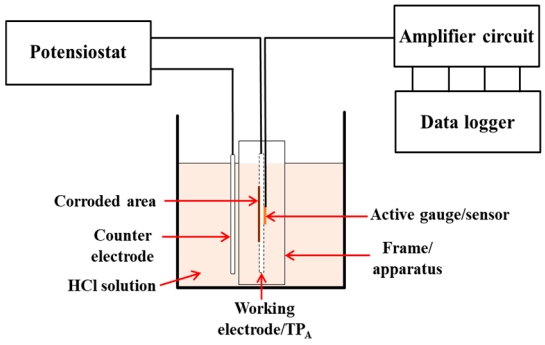

Figure 7. Experimental setup for measuring the thinning of a test piece by galvanostatic electrolysis.

2.2.6. Strain Due to Temperature Change without Corrosion

To investigate the effect of environmental temperature drift on the amplifier circuit, the voltage and temperature were measured using the amplifier circuit with an active-dummy before any corrosion occurred. TP_A and TP_D with attached Tokyo Sokki FLA-5-11 strain gauges R_{AA}, R_{DA}, R_{AD}, and R_{DD} were placed in the bending position using the same configuration as Figure 4. Both TP_A and TP_D were placed under the same ambient conditions. The signal and temperature were monitored for 166 h prior to corrosion, with a data sampling interval of 20 min. The ambient temperature was measured by a thermocouple set near the circuit.

3. Results and Discussion

3.1. Master Curve of the Strain-Voltage Relationship

Through the experiment described in Section 2.1, the strain (ε) from the strain measurement device and the voltage (V) from the amplifier circuit were monitored. Figure 8 plots the master curve for strain versus voltage. The graph shows that the amplifier circuit had a linear relationship with the strain via the equation $\varepsilon = -15 + 39V$. The present amplifier circuit, successfully designed by the active-dummy method for the ACM sensor, has a high sensitivity with a slope of 39 $\mu\varepsilon$ for 1 V. This master curve is used in the following section to convert the output voltage of the amplifier circuit to strain.

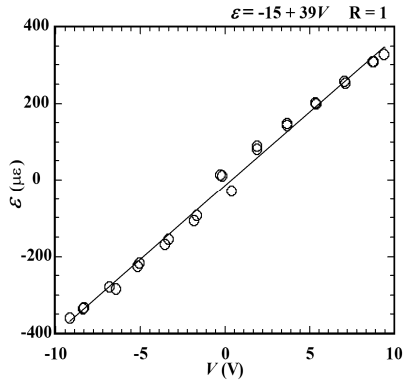

Figure 8. Master curve of strain vs. voltage.

3.2. In Monitoring of Thinning of Test Piece by Galvano Static Electrolysis

The results obtained by the strain gauge of the amplifier circuit for the ACM sensor during galvanostatic electrolysis are shown in Figure 9. Each voltage reading of the amplifier circuit is converted to strain in advance. The figure shows the time evolution of the strain due to the change in thickness of the test piece. When the ACM sensor was immersed in the reservoir, and the surface of the test piece was placed longitudinally, it was easy for making the corrosion products from the surface during the experiment.

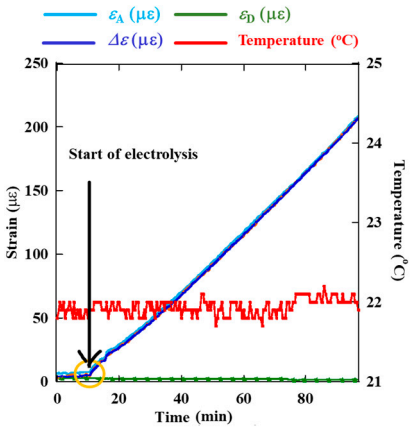

Figure 9. Strain signal pattern as a function of elapsed time during electrolysis process.

The strain of the active circuit (ε_A) had a linear signal in terms of elapsed time during electrolysis. The strain value of the dummy circuit (ε_D) was constant throughout the electrolysis process. $\Delta\varepsilon$ is the difference between ε_A and ε_D, which were obtained by measurements of the amplifier circuit through the active-dummy method for the ACM sensor. $\Delta\varepsilon$ increased linearly with time because given the constant current during the experiment, galvanostatic electrolysis depended on elapsed time. After electrolysis began ε_A is linearly increased this indicated the compressive strain on the test piece, which became smaller with the decreasing of the thickness of test piece according to Equation (1).

Figure 10 shows a close-up of the results around 10.5 min, when electrolysis began. Before 10.5 min, ε_A is constant. After 10.5 min, it is smaller owing to the thinning of the test piece. ε_D is completely unaffected by the signal. It can be concluded that under the active-dummy method, the amplifier circuit for an ACM sensor can measure small values in με, which corresponds to the resolution of the amplifier circuit.

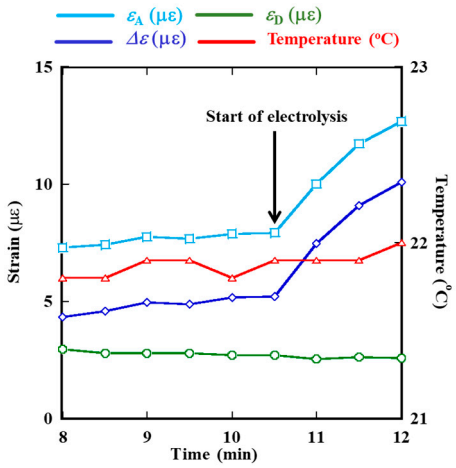

Figure 10. Close-up of Figure 9 around the start of the electrolysis process.

To investigate the accuracy of the amplifier circuit under the active-dummy method, the actual thickness reduction of the test piece was measured. Δy_A is the change in thickness of the test piece, as determined by measuring the actual thickness at five different points on the corroded area of the test piece with a micrometer before and after the experiment. The measurements of the actual thickness were 0.29, 0.28, 0.28, 0.27, and 0.28 mm. The average thickness of the test piece after corrosion was 0.28 mm. Since the initial thickness was 0.48 mm, Δy_A was 0.20 mm.

ΔW is the change in weight of the test piece, as determined from the actual weights measured before and after the experiment and by using the relationship:

$$\Delta y_W = \frac{\Delta W}{S\,d} \tag{4}$$

where ΔW is the change in weight, S is the corroded area of the test piece, and d is the density of the test piece. In this study, ΔW = 1.42 g, S = 900 mm^2, and d = 0.0078 g·mm^{-3}. Furthermore, Δy was obtained via the relationship between Δy and $\Delta\varepsilon$, as described in Section 2.1. The measurement results obtained through the calculations of the actual thickness and actual weight of the test piece are arranged in Table 2. Δy was well aligned with Δy_A and Δy_W, since the errors in the error in these to latter measurements were approximately 12%.

Table 2. Determination of thickness reduction from measured strain, thickness, and weight.

Parameters of Thickness Reduction	Δy	Δy_A	Δy_W
Thickness (μm)	177	200	202
Error (%)	-	11	12

3.3. Strain Due to the Temperature Change of Measurement Environment

Figure 11 shows the original experiment results starting 166 h before corrosion, as described in Section 2.2.6. It is seen that ε_A and ε_D have a similar response to temperature variation. When only the active circuit is used, the variation in ε_A is high, at about 30 με. The dummy circuit can compensate for the variation by subtracting the same response signal as $\Delta\varepsilon$. The variation in $\Delta\varepsilon$ with temperature is small, at less than 10 με. To obtain a more accurate and constant value for $\Delta\varepsilon$, the relationship between temperature and $\Delta\varepsilon$ was adjusted.

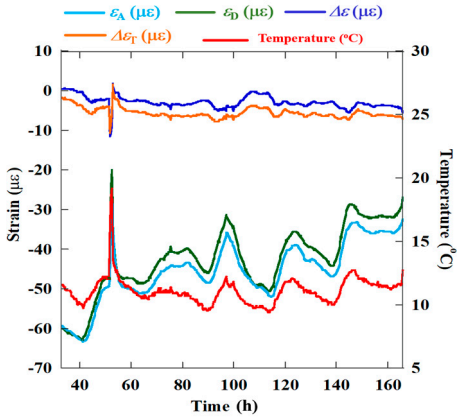

Figure 11. Signal pattern before corrosion is applied.

In Figure 12, the effect of temperature on Δε follows the equation of the master curve $\Delta\varepsilon = 4.68 - 0.68T$. This means that temperature shifts Δε by about 0.68 με/°C. By using this equation, Δε was corrected to reduce the effect of the temperature of the measurement environment.

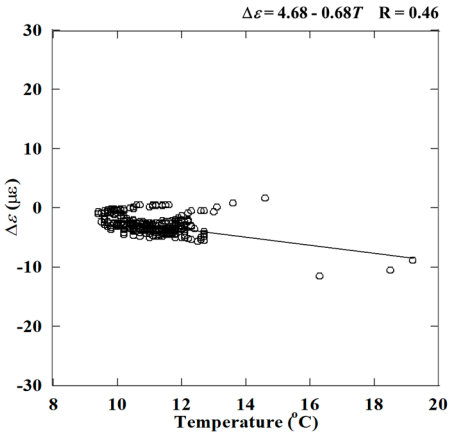

Figure 12. Relationship between the voltage and temperature.

$\Delta\varepsilon_T$ is the signal of Δε obtained after the equation for the relationship between temperature and Δε was applied. The value of $\Delta\varepsilon_T$ is more constant than Δε.

Furthermore, a moving average analysis was conducted. Corrosion is not a rapid process, rather it occurs over long time spans. A moving average analysis, which enables long-time-span analysis of signals, serves to distribute the data. Indeed, as the results in Figure 13 show, the signal obtained is smoother and more constant than the original results.

Figure 13 shows the moving average analysis of the signal pattern of strain using 100 interval data. ε_{AM} is the strain of the active circuit after the moving average analysis, and ε_{DM} is the strain of the dummy circuit after the moving average analysis. $\Delta\varepsilon_M$ is the strain of the amplifier circuit after the moving average analysis, which is obtained from the difference between ε_{DM} and ε_{AM}. From Figure 13, $\Delta\varepsilon_M$ is significantly more constant than $\Delta\varepsilon_T$. This indicates that the moving average is needed in this experiment for accurate measurement without the effect of the temperature variation of the measurement environment.

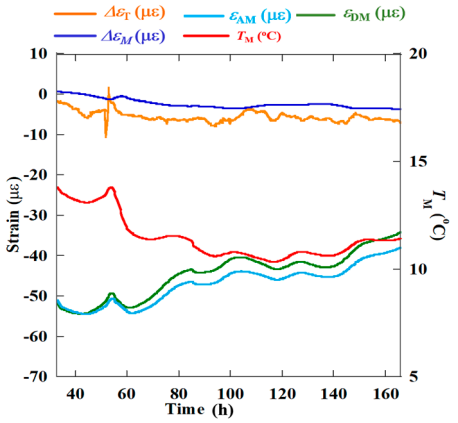

Figure 13. Signal pattern of the voltage before corrosion is applied with the moving average.

4. Conclusions

The conclusions of the present study are as follows:

- An amplifier circuit using the active-dummy method for an ACM sensor based on strain measurement was developed. It successfully overcomes the noise from the environment by compensating from the dummy circuit to the active circuit.
- The master curve of strain versus voltage for the newly developed amplifier circuit indicated high sensitivity with a slope of 39 $\mu\varepsilon/V$.
- The experiment on the thickness reduction of the test piece by galvanostatic electrolysis revealed strong alignment between the calculated results and the strain measurements made with the amplifier circuit by using the active-dummy method. The error rate was approximately 12%.
- The strain due to temperature variation was obtained via $\Delta\varepsilon = 4.68 - 0.68T$. The effect of temperature on $\Delta\varepsilon$ was around 0.68 $\mu\varepsilon/^{\circ}C$.
- $\Delta\varepsilon_T$ remained slightly more constant than $\Delta\varepsilon$ with temperature variations in the measurement environment.
- $\Delta\varepsilon_M$ was significantly more constant than $\Delta\varepsilon_T$, which indicated that the moving average should be used in experiments to obtain more accurate measurements.
- In the field measurement, the corrosion layers of the test piece of the ACM sensor might affect the signals, and its effect would benefit from further study. The relationship of corrosion progression and strain measurement need to be further verified in the future. After developing the ACM sensor system, including an amplifier circuit using the active-dummy method, and unveiling the effect of corrosion layers on the signal, atmospheric corrosion of steel structures can be estimated with an ACM sensor system. The ACM sensor can be installed on different surfaces of the structure.

Acknowledgments: This work was supported by a Grant-in-Aid for Scientific Research (B) JSPS KAKENHI Grant No. 16H03132 and Yokohama National University. In addition, the authors would like to thank the Indonesian Directorate General of Higher Education for their financial support of the author's study.

Author Contributions: Hiroshi Kihira devised the main conceptual ideas; Naoya Kasai, Hiroshi Kihira and Shinji Okazaki developed the theory and proofs for the outline; Naoya Kasai encouraged Nining Purwasih to investigate and supervised the findings of this work; and Nining Purwasih, Naoya Kasai and Shinji Okazaki designed the model and performed the experiments and analyzed the data. All authors discussed the result and contributed to the final manuscript.

Conflicts of Interest: The authors declare there is no conflict of interest. The supporters did not have a role in the design of the study; in the collection, analyses, and interpretation of data; in the writing of the manuscript, or in the decision to publish the results.

Abbreviations

The following abbreviations are used in this manuscript.

D	Density of test piece ($g \cdot cm^{-3}$)
$d\theta$	Center angle of curvature of the test piece (°)
E	Young's modulus of the test piece (Pa)
R_{AA}	Resistance of active gauge for active circuit (Ω)
R_{AD}	Resistance of active gauge for dummy circuit (Ω)
R_{DA}	Resistance of dummy gauge for active circuit (Ω)
R_{DD}	Resistance of dummy gauge for dummy circuit (Ω)
R_{VR}	Resistance of variable resistor (Ω)
S	Corroded area of test piece (cm^2)
S_G	Strain gauge for measuring the strain by commercial strain (-)
T	Temperature (°C)
T_M	Temperature with moving average analysis (°C)
V_A	Output voltage of active circuit (V)
V_{BA}	Output voltage of bridge circuit of active circuit (mV)
V_{BD}	Output voltage of bridge circuit of dummy circuit (mV)
V_{CC}	Positive input voltage for op-amp (V)
V_D	Output voltage of dummy circuit (V)
V_{EE}	Negative input voltage for op-amp (V)
V_{IN}	Input voltage for bridge circuit (V)
$V_{p\text{-}p}$	Peak-to-peak voltage (V)
Y	Test piece thickness (m)
ΔV	Difference between the output voltages of the active and dummy circuits (V)
ΔW	Actual weight obtained by analysis (g)
Δy	Change in thickness of test piece (m)
Δy_A	Actual thickness obtained by analysis (μm)
Δy_W	Actual thickness obtained by electrochemical analysis (μm)
$\Delta\varepsilon$	Differential strain (με)
$\Delta\varepsilon_M$	Differen ce in strain between the active and dummy circuits, determined by moving average analysis (με)
$\Delta\varepsilon_T$	Difference in strain, taking account of the temperature effect (με)
ε	Strain in test piece (-)
ε_A	Strain of the active circuit (με)
ε_{AM}	Strain of the active circuit obtained by moving average analysis (με)
ε_{AT}	Strain of active circuit, taking account of the temperature effect (με)
ε_D	Strain of dummy circuit (με)
ε_{DM}	Strain of dummy circuit obtained by moving average analysis (με)
ε_{DT}	Strain of dummy circuit, taking account of temperature effect (με)
ε_m	Strain with input only from signal (-)
$\varepsilon_{m,t,o}$	Strain with input from signal and environmental factors (-)
$\varepsilon_{t,o}$	Strain with input only from environmental factors (-)
ρ	Radius of curvature of test piece (m)
σ_y	Yield stress of test piece (Pa)

References

1. Alamin, M.; Tian, G.Y.; Andrews, A.; Jackson, P. Corrosion detection using low-frequency RFID technology. *Insight-Non-Destr. Test. Cond. Monit.* **2012**, *54*, 72–75. [CrossRef]
2. Zhang, H.; Yang, R.; He, Y.; Tian, G.Y.; Xu, L.; Wu, R. Identification and characterization of steel corrosion using passive high frequency RFID sensors. *Measurement* **2016**, *92*, 421–427. [CrossRef]
3. Zhang, J.; Tian, G.Y.; Marindra, A.M.J.; Sunny, A.I.; Zhao, A.B. A review of passive RFID tag antenna-based sensors and systems for structural health monitoring applications. *Sensors* **2017**, *17*, 265. [CrossRef] [PubMed]
4. Gattan, S.K.T.; Taylor, S.E.; Sun, T.; Basheer, P.A.M.; Grattan, K.T.V. Monitoring of corrosion in structural reinforcing bars: Performance comparison using in situ fiber-optic and electric wire strain gauge systems. *IEEE Sens. J.* **2009**, *9*, 1494–1502. [CrossRef]

5. Hu, W.; Cai, H.; Yang, M.; Tong, X.; Zhou, C.; Chen, W. Fe-C-coated fibre Bragg grating sensor for steel corrosion monitoring. *Corros. Sci.* **2011**, *53*, 1933–1938. [CrossRef]
6. Zang, N.; Chen, W.; Zheng, X.; Hu, W.; Gao, M. Optical sensor for steel corrosion monitoring based on etched Fiber Bragg Grating sputtered with iron film. *IEEE Sens. J.* **2015**, *15*, 3511–3556.
7. Al Handawi, K.; Vahdati, N.; Rostron, P.; Lawand, L.; Shiryayev, O. Strain based FBG sensor for real-time corrosion rate monitoring in pre-stressed structures. *Sens. Actuator B* **2016**, *236*, 276–285. [CrossRef]
8. Almubaied, O.; Chai, H.K.; Islam, M.R.; Lim, K.; Tan, C.G. Monitoring corrosion process of reinforced concrete structure using FBG strain sensor. *IEEE Trans. Instrum. Meas.* **2017**, *66*, 2148–2155. [CrossRef]
9. Mansfeld, F.; Kenkel, J.V. Electrochemical monitoring of atmospheric corrosion phenomena. *Corros. Sci.* **1976**, *16*, 111–112. [CrossRef]
10. Mansfeld, F.; Tsai, S. Laboratory studies of atmospheric corrosion—I. Weight loss and electrochemical measurements. *Corros. Sci.* **1980**, *20*, 853–872. [CrossRef]
11. Ridha, M.; Fonna, S.; Huzni, S.; Supardi, J.; Ariffin, A.K. Atmospheric corrosion of structural steels exposed in the 2004 tsunami-affected areas of Aceh. *IJAME* **2013**, *7*, 1014–1022. [CrossRef]
12. Monsada, A.M.; Margarito, M.T.; Milo, L.C.; Casa, E.P.; Zabala, J.V.; Maglines, A.S.; Basilia, B.A.; Harada, S.; Shinohara, T. Atmospheric corrosion exposure study of The Philippine Historical all steel Basilica. *Zairyo Kankyo* **2016**, *C-107*, 267–270.
13. Dara, T.; Shinohara, T.; Umezawa, O. The Behavior of corrosion of low carbon steel affected by corrosion product and Na_2SO_4 concentration under artificial rainfall test. *Zairyo Kankyo* **2016**, *C-114*, 298–302.
14. Lien, L.T.H.; Hong, H.L.; San, P.T.; Hieu, N.T.; Nga, N.T.T. Atmospheric corrosion of carbon steel and weathering steel—Relation of corrosion and environmental factors. *Zairyo Kankyo* **2016**, *C-110*, 280–284.
15. Odara, T.; Tahara, A.; Dara, T. Atmospheric corrosion behaviors of steels in Japan. *Zairyo Kankyo* **2016**, *C-111*, 285–288.
16. Viyanit, E.; Pongsaksawad, W.; Sorachot, S.; Matsuyama, H.; Fukuda, N. Investigation of atmospheric corrosion behavior of austenitic and ferritic stain less steel welds under tropical climate of Thailand. *Zairyo Kankyo* **2016**, *C-109*, 275–279.
17. Mansfeld, F.; Jeanjaquet, S.L.; Kendig, M.W.; Roe, D.K. A new atmospheric corrosion rate monitor development and evaluation. *Atmos. Environ.* **1986**, *20*, 1179–1192. [CrossRef]
18. Nishikata, A.; Yamashita, Y.; Katayama, H.; Tsuru, T.; Usami, A.; Tanabe, K.; Mabuchi, H. An electrochemical impedance study on atmospheric corrosion of steels in a cyclic wet–dry condition. *Corros. Sci.* **1995**, *37*, 2059–2069. [CrossRef]
19. Nishikata, A.; Suzuki, F.; Tsuru, T. Corrosion monitoring of nickel-containing steels in marine atmospheric environment. *Corros. Sci.* **2005**, *47*, 2578–2588. [CrossRef]
20. Cruz, R.P.V.; Nishikata, A.; Tsuru, T. AC impedance monitoring of pitting corrosion of stainless steel under a wet–dry cyclic condition in chloride-containing environment. *Corros. Sci.* **1996**, *38*, 1397–1406. [CrossRef]
21. El-Mahdy, G.A.; Nishikata, A.; Tsuru, T. Electrochemical corrosion monitoring of galvanized steel under cyclic wet–dry conditions. *Corros. Sci.* **2000**, *42*, 183–194. [CrossRef]
22. Yadav, A.P.; Nishikata, A.; Tsuru, T. Electrochemical impedance study on galvanized steel corrosion under cyclic wet–dry conditions-influence of time of wetness. *Corros. Sci.* **2004**, *46*, 169–181. [CrossRef]
23. Yadav, A.P.; Suzuki, F.; Nishikata, A.; Tsuru, T. Investigation of atmospheric corrosion of Zn using ac impedance and differential pressure meter. *Electrochim. Acta* **2004**, *49*, 2725–2729. [CrossRef]
24. El-Mahdy, G.A.; Nishikata, A.; Tsuru, T. AC impedance study on corrosion of 55% Al–Zn alloy-coated steel under thin electrolyte layers. *Corros. Sci.* **2000**, *42*, 1509–1521. [CrossRef]
25. Dong, J.H.; Chen, W.; Ke, W. Corrosion evolution of steel simulated of SO_2 polluted coastal atmospheres, Zairyo Kankyo 2016, C-112, 289–292. *Zairyo Kankyo* **2016**, *C-112*, 289–292.
26. Thee, C.; Dong, J.; Ke, W. Corrosion monitoring of weathering steel in a simulated coastal-industrial environment. *Int. J. Environ. Chem. Ecol. Geol. Geophys. Eng.* **2015**, *9*, 587–593.
27. Parson, N.; Khamsuk, P.; Sorachot, S.; Khonraeng, W.; Wongpinkaew, K.; Kaewkumsai, S.; Pongsaksawad, W.; Viyanit, E.; Chianpairot, A. Atmospheric corrosion of structural steels in Thailand Tropical Climate. *Zairyo Kankyo* **2016**, *C-108*, 271–274.
28. Li, C.; Ma, Y.; Li, Y.; Wang, F. EIS monitoring study of atmospheric corrosion under variable relative. *Corros. Sci.* **2010**, *52*, 3677–3686. [CrossRef]

29. Shitanda, I.; Okumura, A.; Itagaki, M.; Watanabe, K.; Asano, Y. Screen-printed atmospheric corrosion monitoring sensor based on electrochemical impedance spectroscopy. *Sens. Actuators B* **2009**, *139*, 292–297. [CrossRef]
30. Cai, J.P.; Lyon, S.B. A mechanistic study of initial atmospheric corrosion kinetics using electrical resistance sensor. *Corros. Sci.* **2005**, *47*, 2956–2973. [CrossRef]
31. Li, S.; Kim, Y.G.; Jung, S.; Song, H.S.; Lee, S.M. Application of steel thin film electrical resistance sensor for in situ corrosion monitoring. *Sens. Actuators B* **2007**, *120*, 368–377. [CrossRef]
32. He, Y.; Tian, G.; Zhang, H.; Alamain, M.; Simm, A.; Jackson, P. Steel corrosion characterization using pulsed eddy current systems. *IEEE Sens. J.* **2012**, *12*, 2113–2120. [CrossRef]
33. Yasri, M.; Gallee, F.; Lescop, B.; Diler, E.; Thierry, D.; Rioual, S. Passive wireless sensor for atmospheric corrosion monitoring. In Proceedings of the 8th European Conference on Antennas and Propagation (EuCAP), The Hague, The Netherlands, 6–11 April 2014; pp. 2945–2949.
34. Lin, A.N.; Saito, R.; Takaya, S.; Miyagawa, T. *Determination of Young's Modulus of Rush-Layer by Bending Experiment*; Technical Paper; JCI: Tokyo, Japan, 2013; Volume 35, pp. 1117–1122.
35. Kasai, N.; Hiroki, M.; Yamada, T.; Kihira, H.; Matsuoka, K.; Kuriyama, Y.; Okazaki, S. Atmospheric corrosion sensor based on strain measurement. *Meas. Sci. Technol.* **2017**, *28*, 15106. [CrossRef]
36. Kasai, N.; Utatsu, K.; Park, S.; Kitsukawa, S.; Sekine, K. Correlation between corrosion rate and AE signal in an acidic environment for mild steel. *Corros. Sci.* **2009**, *51*, 1679–1684. [CrossRef]